Ocean Engng, Vol. 17, No 1/2, pp. 125–154, 1990.
Printed in Great Britain.

0029–8018/90 $3.00 + .00
Pergamon Press plc

DIFFRACTED WAVE FIELD AND DYNAMIC PRESSURES AROUND A VERTICAL CYLINDER

V. SUNDAR, S. NEELAMANI and C. P. VENDHAN
Ocean Engineering Centre, Indian Institute of Technology, Madras, India

Abstract—Investigations on the hydrodynamic pressures due to regular and random waves exerted on a large vertical cylinder in a constant water depth are reported in this paper. In the experimental investigation, the test cylinder embedded with diaphragm-type pressure transducers at nine different elevations was rotated about its axis to measure the dynamic pressure around its circumference. The wave field in the neighbourhood of the cylinder was measured at six different locations. The results of the experiments are compared with the linear diffraction theory of MacCamy, R. C. and Fuchs, R. A. [(1954) Wave forces on piles: a diffraction theory. U.S. Army Beach Erosion Board, Technical Memorandum No. 69]. In general, the agreement between the theoretical and experimental results is found to be satisfactory. A comparison between the regular and random wave test results is also presented and discussed.

1. INTRODUCTION

THE CONTINUING search for offshore oil and gas resources has driven mankind into deeper waters of the oceans, where the design of offshore structures subjected to waves become quite complicated due to the hostile environment. Accurate assessment of not only the total wave loads but also the wave-induced sectional forces and dynamic pressures are essential to optimise the design of such structures. The evaluation of wave forces on vertical cylinders has been the subject of intensive research during the last few decades.

The first empirical formulation for the calculation of wave forces on slender members ($D/L < 0.2$, where D is the diameter of the cylinder and L is wave length) was proposed by Morison *et al.* (1950), based on the assumption that the presence of the structure does not affect the characteristics of the incident wave field. This formulation, however, fails to predict the wave loads accurately, for $D/L > 0.2$ due to the dominant wave diffraction.

The scattering of waves from a fixed body was first recognised by Havelock (1940), and based on which, MacCamy and Fuchs (1954) proposed a closed form solution to evaluate the hydrodynamic pressures, forces and moments on a large vertical cylinder in regular waves. While considerable work has been reported on the total wave forces on vertical cylinders, studies on wave-induced dynamic pressures are rather limited. Notable contributions on the dynamic pressures on vertical cylinders due to regular waves are those of Laird (1955), Priest (1962), Chakrabarti and Tam (1975), Endo and Tosaka (1985) and Chakrabarti *et al.* (1986). The results were presented in a variety of forms as a function of flow parameters. Hellstorm and Rundgren (1954) have attempted to correlate the measured dynamic pressures around a cylindrical model with the theoretical pressures on a plane vertical wall. Nakamura (1976) has measured the dynamic pressures exerted on a cooling water intake structure on the coast of the Pacific

Ocean and concluded that the measured pressures due to irregular waves were found to be smaller in the deeper part and larger near the still water level (S.W.L) than those given by the MacCamy and Fuchs (1954) linear diffraction theory. Caveleri *et al.* (1977) have measured pressure fluctuations due to surface waves at different elevations on a tower in the Adriatic Sea near Venice and found that the measured pressures deviate from the linear wave theory. The deviation was observed to be greater at lower frequencies and with the increase in the depth of measurement of the dynamic pressures.

Raman and Rao (1983) have measured the dynamic pressures due to laboratory wind-generated waves at three different elevations below the S.W.L. The experimental results were compared with the MacCamy and Fuchs linear diffraction theory. It was noticed in their study that the measured pressures of the pressure ports facing the side wall deviated considerably from the MacCamy and Fuchs linear diffraction theory. This phenomenon was attributed to the proximity of the flume side wall. The correlation between the measured and theoretical pressures for the other pressure transducer orientation with respect to the wave direction was found to be quite satisfactory at z/d (where z is the point of pressure measurement, measured negative downwards from S.W.L., and d is the water depth) of -0.22 and -0.44. It should be noted that the frequency range adopted covers mostly the shallow and intermediate water depth conditions. However, significant deviations were observed between the measured and theoretical values with increase in the depth of measurement of the dynamic pressures, similar to the observations of Caveleri *et al.* (1977).

A review of the existing literature reveals that only limited work has been reported on the wave-induced dynamic pressures on vertical cylinders, of which most of the work pertains to the action of regular waves. As for the literature on the study of dynamic pressures on vertical cylinders due to random waves, Nakamura (1976) has carried out field experiments, whereas Raman and Rao (1983) have investigated the random pressures on model cylinders exposed to laboratory wind-generated waves. Apart from the above, to the best of the author's knowledge, there does not seem to be any other published work related to dynamic pressures on vertical cylinders due to random waves.

The measurement of the wave-induced dynamic pressures around the circumference of a large vertical cylinder would be needed for a more rigorous verification of the linear wave theory, rather than the measurement of the total wave force. Further, the inevitable side wall effects on the wave diffraction due to the presence of large diameter structures in the narrow laboratory wave flumes can be inferred from the measurement of dynamic pressures around a cylindrical structure. The study of the diffracted wave field around a large vertical cylinder would be useful in fixing the minimum air gap between the mean sea level and the deck of the offshore structures. The above reasons prompted the investigators to carry out a detailed investigation on the dynamic pressure around a large vertical cylinder and the diffracted wave field subjected to random waves.

2. THEORETICAL CONSIDERATIONS

2.1. *Linear diffraction theory*

The hydrodynamic pressure, $p(t)$ on a large diameter vertical cylinder and the diffracted water surface elevation, $\eta_r(t)$ at any radial distance r, at time t are given by MacCamy and Fuchs (1954) as

$$p(t) = \frac{\rho g H \cosh[k(d+z)]}{\pi ka \cosh(kd)} \sum_{m=0}^{\infty} \frac{\epsilon_m i^m}{H_m^{(1)'}(ka)} \cos[m(\pi-\theta)] \in^{-i\alpha t} \quad (1)$$

and

$$\eta_r(t) = \frac{H}{2} \sum_{m=0}^{\infty} \epsilon_m i^{m+1} \left[J_m(kr) - \frac{J_m'(ka)}{H_m^{(1)'}(ka)} H_m^{(1)}(kr) \right] \cos[m(\pi-\theta)] \in^{-i\alpha t} \quad (2)$$

in which ρ = the mass density of water, g = the acceleration due to gravity, k = the wave number $(2\pi/L)$, α = the angular wave frequency $(2\pi f)$, where f = the linear wave frequency, a = the cylinder radius, J_m = the Bessel function of the first kind of order m, $H_m^{(1)}$ = the Hankel function of first kind of order m, prime denoting the derivative of the functions with respect to their arguments, ϵ_m = constants with $\epsilon_0 = 1$ and $\epsilon_m = 2$ for $m \geq 1$, and θ = the polar angle measured clockwise from the leading edge on the circumference of the cylinder (thus $\theta = 180°$ refers to the trailing edge) (Fig. 1).

The transfer function for dynamic pressures on a vertical cylinder, $TF_{pr}(f)$ and that for the diffracted water surface elevation, $TF_{rr}(f)$ can be obtained from the above two equations as

$$TF_{pr}(f) = \frac{2\rho g}{\pi ka} \frac{\cosh[k(d+z)]}{\cosh(kd)} \sum_{m=0}^{\infty} \frac{\epsilon_m i^m}{H_m^{(1)'}(ka)} \cos[m(\pi-\theta)] \quad (3)$$

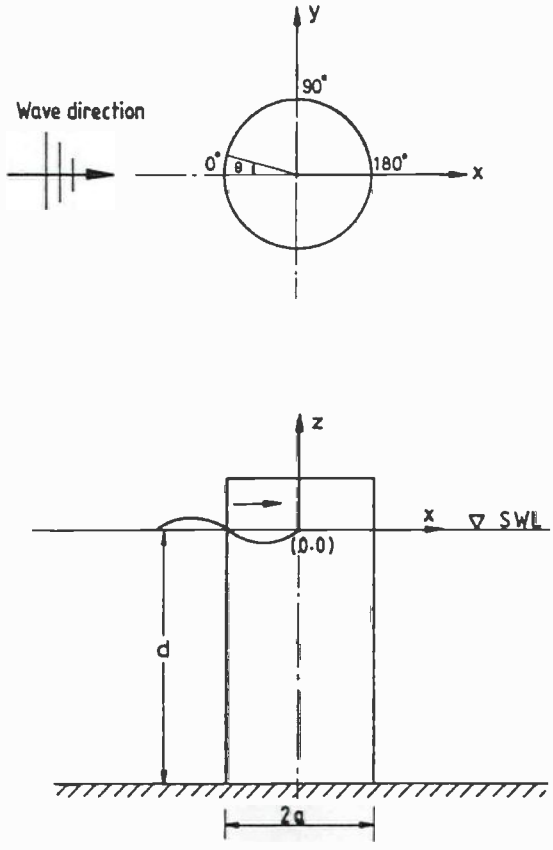

FIG. 1. Definition sketch.

and

$$TF_{rt}(f) = \sum_{m=0}^{\infty} \epsilon_m i^{m+1} \left[J_m(kr) - \frac{J'_m(ka)}{H_m^{(1)'}(ka)} H_m^{(1)}(kr) \right] \cos[m(\pi - \theta)]. \tag{4}$$

The spectral density of the dynamic pressure, $S_{pt}(f)$ and the diffracted water surface elevation, $S_{rt}(f)$ can now be expressed as

$$S_{pt}(f) = |TF_{pt}(f)|^2 S_{\eta\eta}(f) \tag{5}$$

and

$$S_{rt}(f) = |TF_{rt}(f)|^2 S_{\eta\eta}(f) \tag{6}$$

in which $S_{\eta\eta}(f)$ = the spectral density of the incident water surface elevation, η.

2.2. *Average pressure coefficient over the frequency domain*

Let the pressure spectrum be approximated as

$$S_{pt}(f) = (C_p \rho g)^2 S_{\eta\eta}(f) + \epsilon \tag{7}$$

where C_p is a pressure coefficient uniform over f. Minimising the error ϵ over the frequency range of interest in a least-square sense, one has

$$(C_p \rho g)^2 = \frac{\sum S_{pm}(f) S_{\eta\eta}(f)}{\sum S_{\eta\eta}^2(f)} \tag{8}$$

where S_{pm} is the measured pressure spectral density value. The pressure coefficient C_p as defined above may be obtained for different input parameters, namely H_s and f_0. Then, given a wave spectrum defined by a particular H_s and f_0, one can directly choose an appropriate value for C_p. It will be of interest to compare C_p from Equation (8) with the pressure coefficient for an appropriate regular wave.

3. EXPERIMENTAL INVESTIGATIONS

3.1. *Experimental set-up*

The experimental investigations were carried out in a 4 m wide and 45 m long wave flume at the Ocean Engineering Centre, Indian Institute of Technology, Madras, India. The water depth throughout the experiments was maintained constant at 2.5 m. Random waves were generated using a twin flap wave maker located at one end of the flume and its movement is controlled by a computer. A suitable wave absorber is provided at the other end of the flume to absorb effectively the incident wave energy. The test model used for the present study is a PVC pipe of diameter 400 mm and wall thickness of 15 mm, fixed at a distance of 20 m from the wave maker. Nine diaphragm-type pressure transducers each of ± 0.5 bar capacity were embedded at different depths of submergence. One among the nine pressure transducers was fixed at the S.W.L. itself to study closely the nonlinear effects. The spacings between the pressure transducers close to the S.W.L. were kept lower than those close to the flume bed, considering the rapid decay of the kinematics of the progressive waves. The details of the test cylinder

are shown in Fig. 2. The cylinder is waterproof and one of its ends is fixed rigidly to the flume bed. A special arrangement at the top of the cylinder is provided to rotate the cylinder about its own vertical axis. This enables any desired angle of orientation of the pressure transducer with respect to the wave direction.

A resistance-type wave probe fixed at a distance of 14 m from the paddle was used to register the time history of the incident wave elevation. Another wave probe fixed around the test model at six different locations registered the time history of the scattered waves. The leads from the pressure transducers and the wave probes were connected to multi-channel carrier frquency amplifiers and wave monitors, respectively, and the signals from this system were acquired continuously using a personal computer. The general instrumentation set-up used for the present study is shown in Fig. 3.

3.2. *Experimental procedure*

The wave probes and the pressure transducers were calibrated prior to and after each set of experiments. The test model was exposed to random waves with Pierson–Moskowitz spectra having a spectral width of $\epsilon_\eta = 0.6$ and two different energy levels. In addition to this, experiments were also conducted for random waves with a narrow band spectrum having $\epsilon_\eta = 0.3$. The characteristics of these generated spectra are displayed in Table 1.

The experimental data were acquired at a sampling rate of 20 samples/sec from each channel for a time span of 51.2 sec. About 45–50 waves were collected at this time span. The test cylinder was rotated about its own vertical axis in steps of 30° from θ = 0 to 180°. In order to carry out a comparative study between regular and random wave tests, the cylinder was also subjected to regular waves of different heights and periods. The wave heights ranged from 3 cm to 25 cm and wave periods ranged from 0.6 to 2.0 sec.

4. RESULTS AND DISCUSSION

4.1. *General*

The time history of the simulated random waves and the corresponding dynamic pressures were analysed and tested for their normality. The instantaneous water surface elevation and the dynamic pressures were found to follow the Gaussian distribution reasonably well. The frequency domain analysis of the measured time series was performed using the FFT technique. The raw spectral estimates were smoothed using the nine point moving average method as proposed by Daemrich *et al.* (1980). The frequency range of the generated wave spectra covered mostly the deep water conditions.

TABLE 1. CHARACTERISTICS OF THE LABORATORY-SIMULATED WAVE SPECTRA

S. No.	Type of spectrum	Significant wave height H_s (cm)	Peak frequency f_0 (Hz)	Spectral width parameter ϵ_η
1	Narrow band	6.6	0.74	0.3
2	PM1	4.46	0.76	0.6
3	PM2	9.25	0.76	0.6

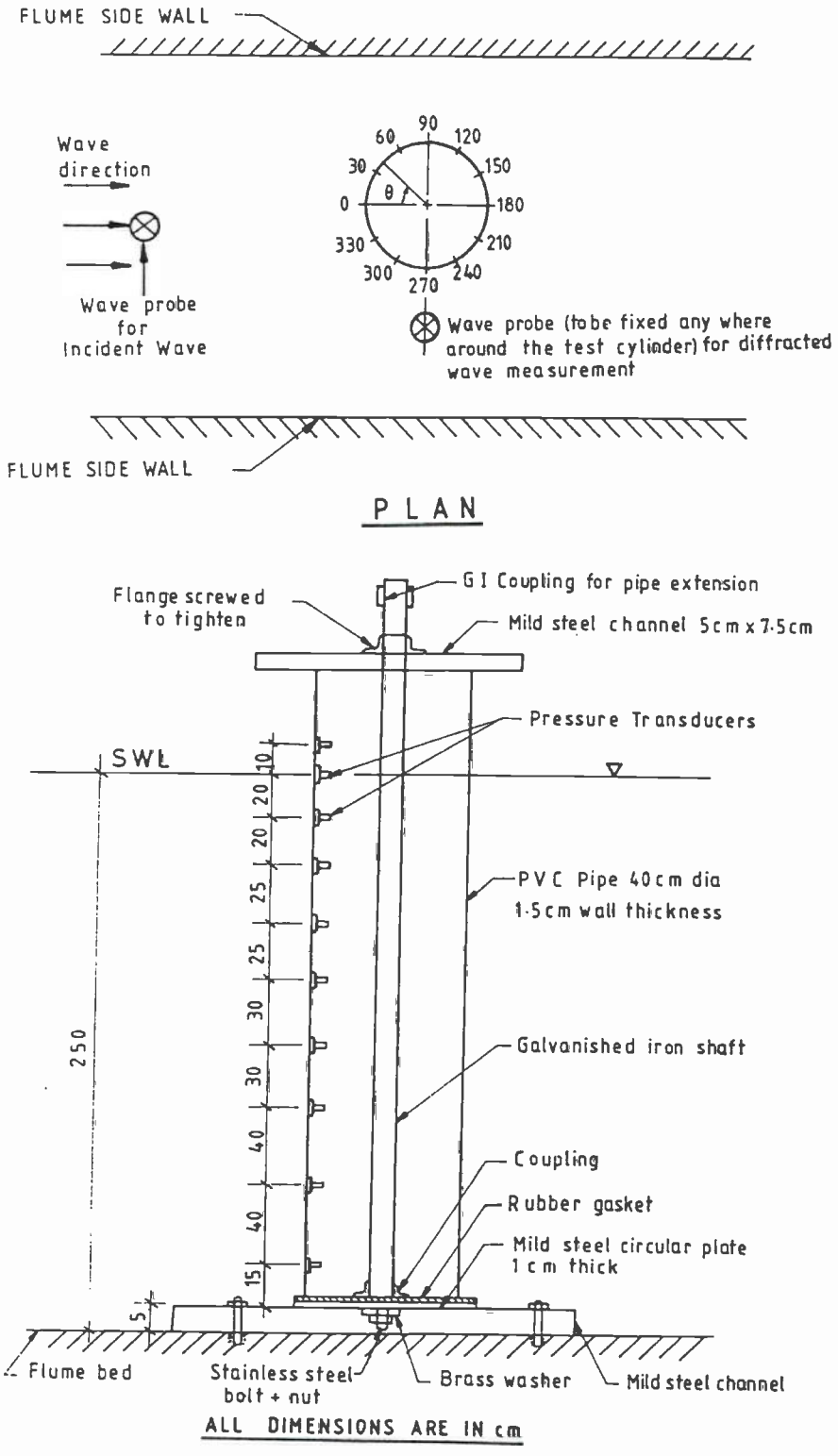

FIG. 2. Experimental set-up.

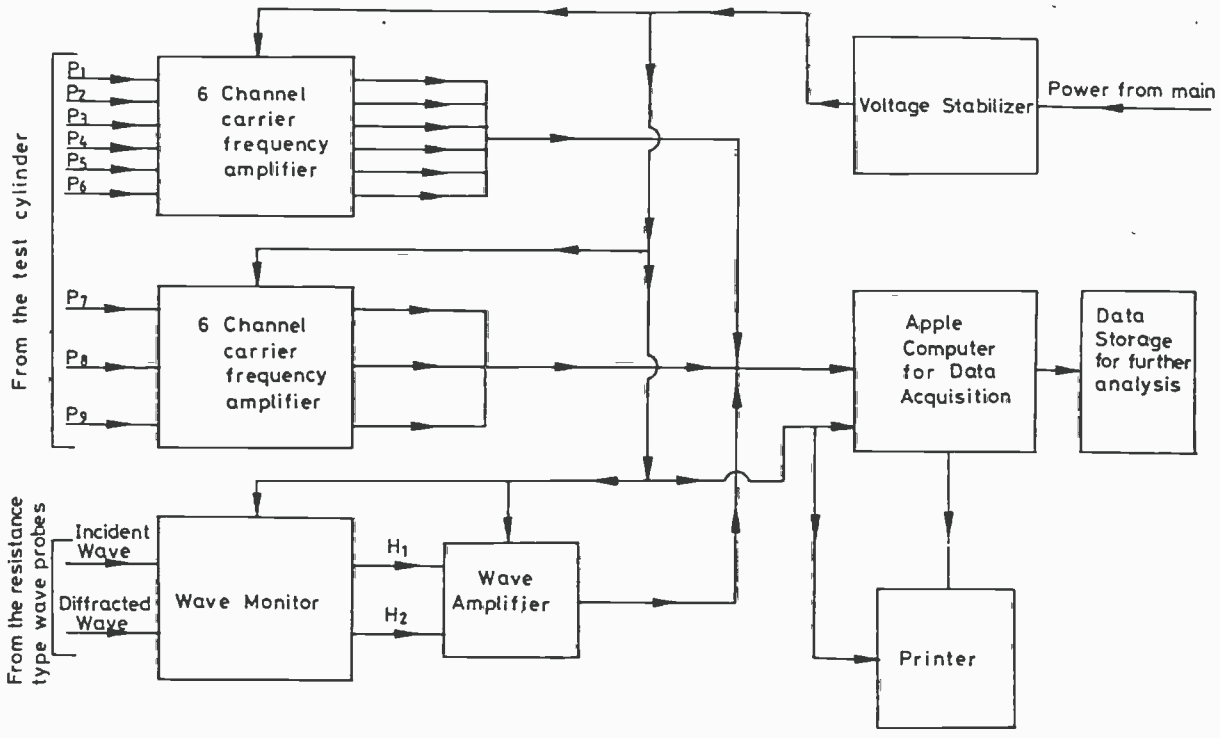

FIG. 3. General instrumentation set-up.

4.2. *Theoretical and measured dynamic pressure spectra*

Though the dynamic pressures exerted on the test cylinder were measured for θ = 0 to 180° in steps of 30°, in order to make the presentation simple, only typical plots showing the comparison between the theoretical and measured pressure spectra for θ = 0°, 90° and 180° for the cases of narrow band and PM2 spectra are shown in Figs 4a–c and Figs 5a–c, respectively. The corresponding incident wave spectrum is also superposed. In general, the correlation between the theory and experiments is found to be satisfactory. It is seen that the agreement between the theory and experiment is good even at S.W.L. for the case of narrow band spectrum, whereas deviations are observed at S.W.L. for the broad band cases, showing that the effect of scattering and nonlinearity is more predominant for a broad band spectrum than for the case of a narrow band spectrum. It is also noticed in these plots that the spectral peaks of both theoretical and measured pressure spectra shift towards the lower frequency zone as the depth of submergence of the pressure transducer increases. This obviously is due to faster decay of the high frequency components with respect to depth. It is also observed that at $z/d = -0.36$, the measured peak pressure spectral value is less than 1% of that measured at S.W.L. Therefore, further results and discussions will only be confined to pressure transducer locations with z/d from 0.0 to -0.26.

4.3. *Measured pressure spectral density around the circumference of the cylinder*

Typical plots showing the variation of the measured pressure spectral density around the circumference of the cylinder for two different z/d values (z/d = 0.0 and -0.08) for the narrow band, PM1 and PM2 cases are shown in Figs 6a–c. It is seen in general

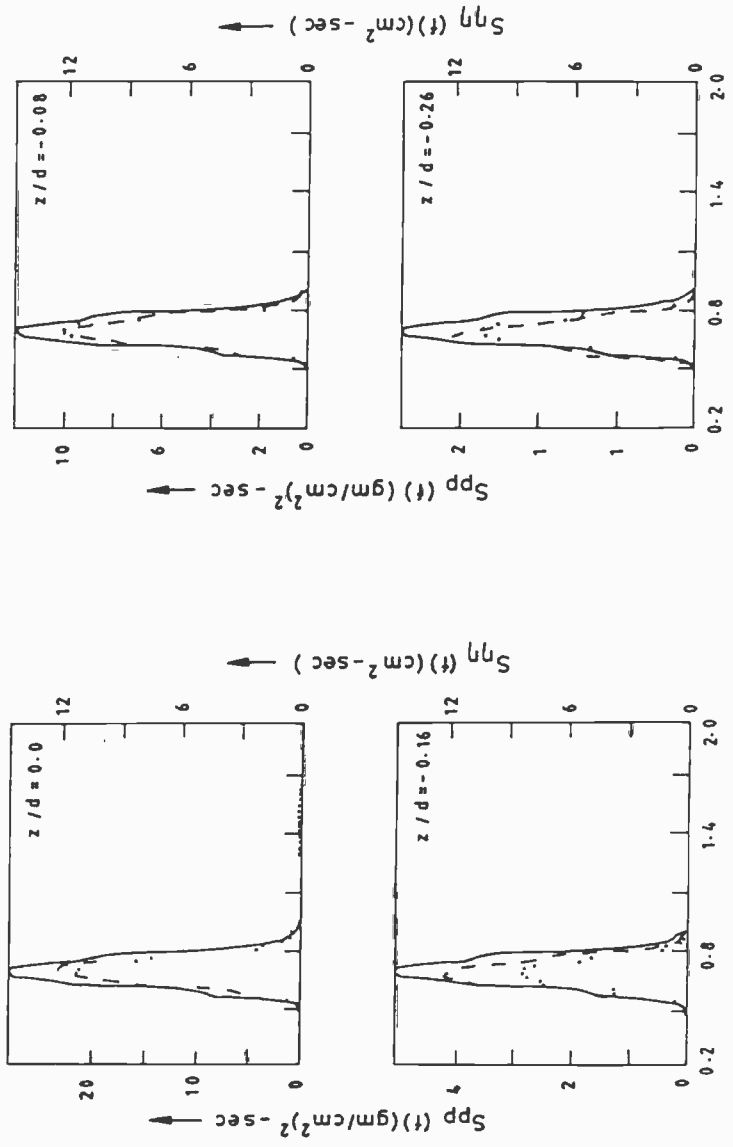

FIG. 4a. Comparison of theoretical and experimental pressure spectrum for $\theta = 0°$.

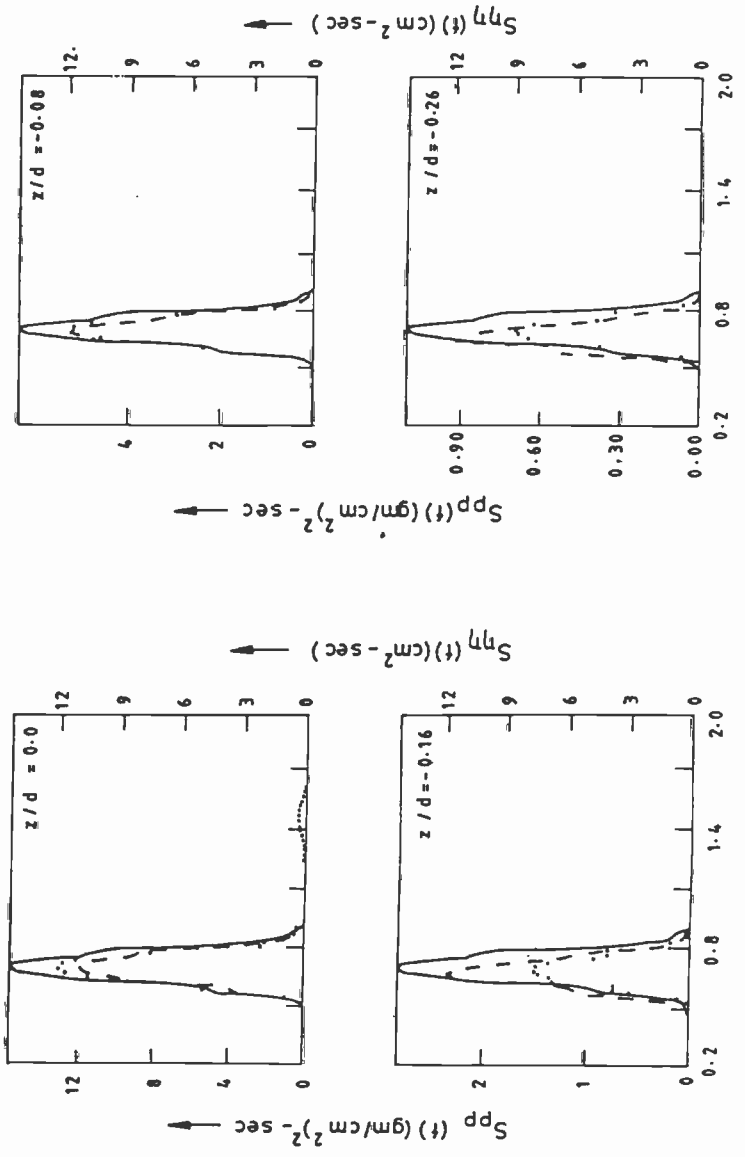

FIG. 4b. Comparison of theoretical and experimental pressure spectrum for $\theta = 90°$.

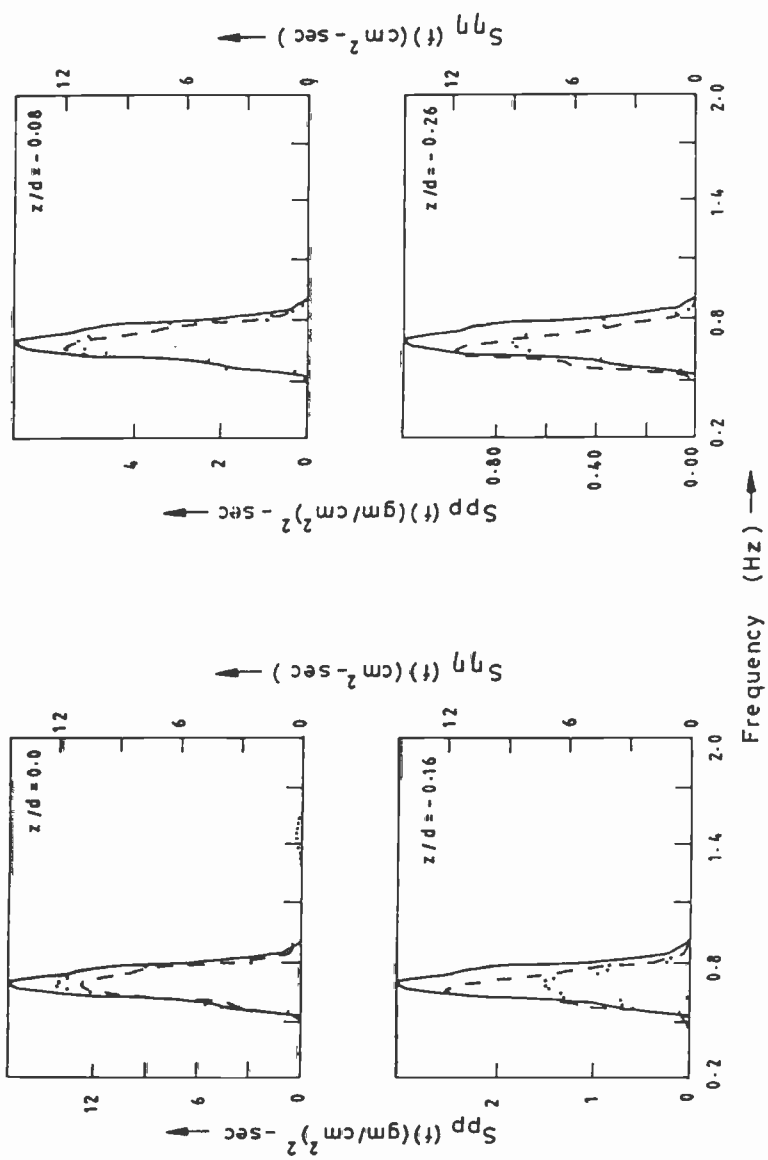

FIG. 4c. Comparison of theoretical and experimental pressure spectrum for $\theta = 180°$.

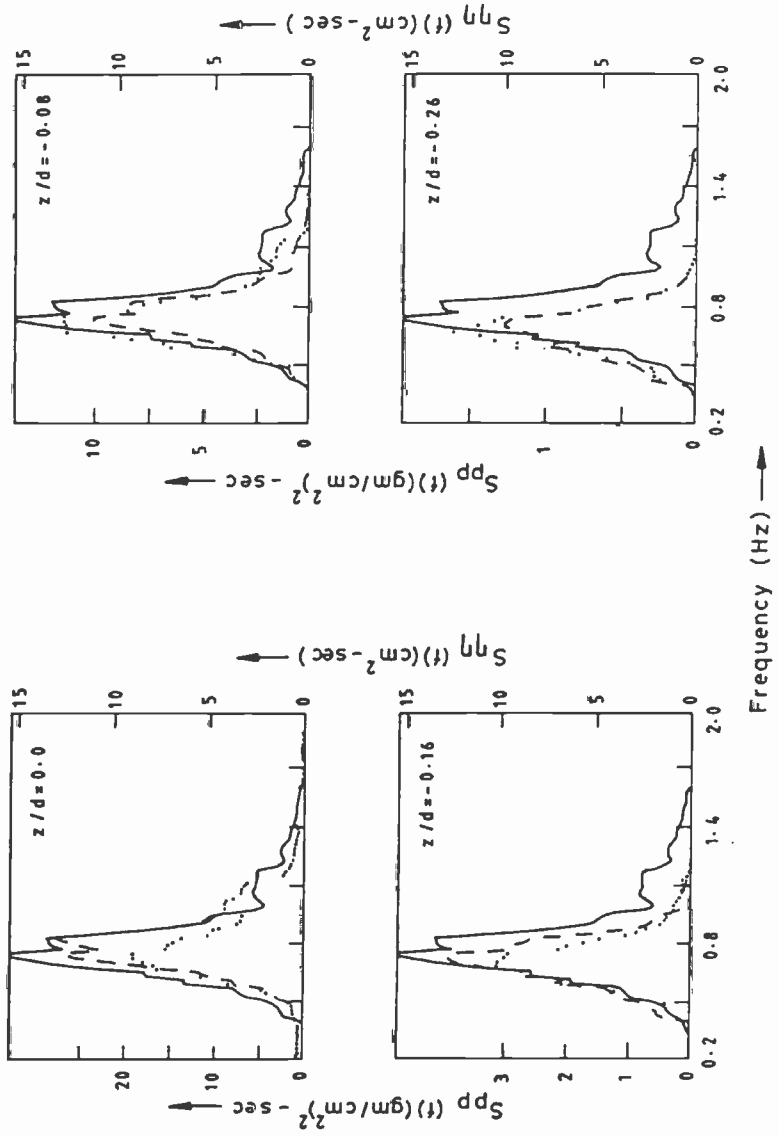

Legend: Exp.(S_{pp}(f)) ·····, Theory(S_{pp}(f))— — —, Wave($S_{\eta\eta}$(f))——

FIG. 5a. Comparison of theoretical and experimental pressure spectrum for $\theta = 0°$.

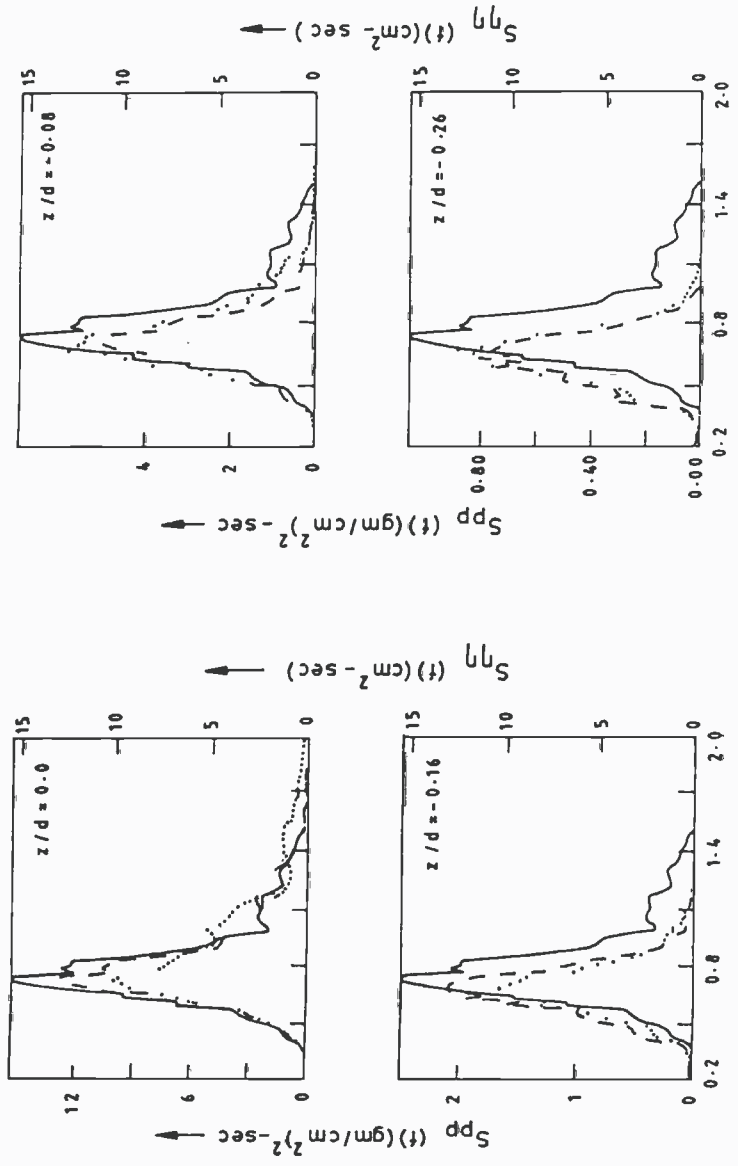

FIG. 5b. Comparison of theoretical and experimental pressure spectrum for $\theta = 90°$.

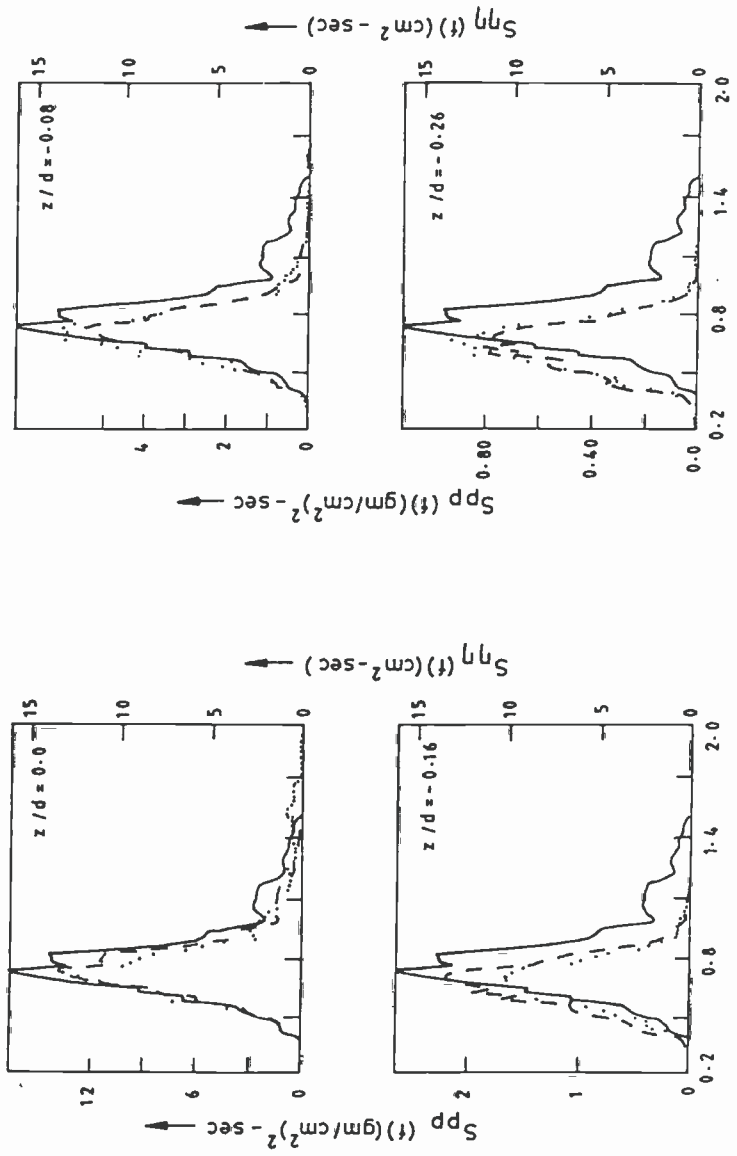

FIG. 5c. Comparison of theoretical and experimental pressure spectrum for $\theta = 180°$.

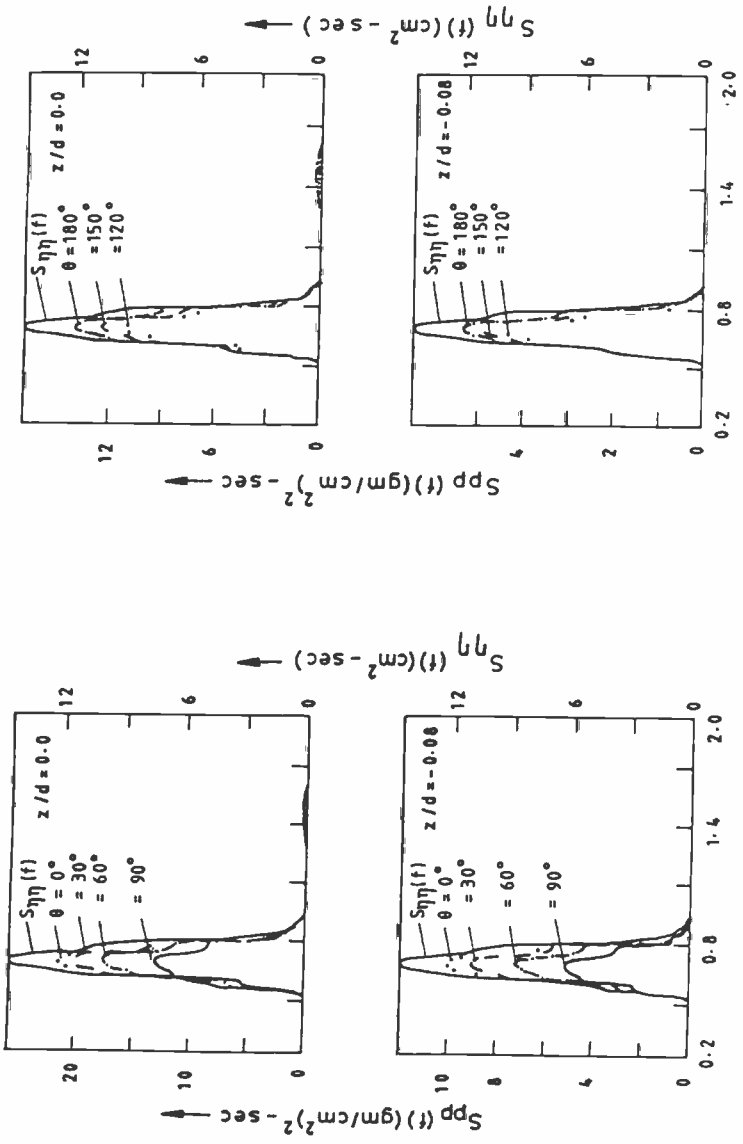

FIG. 6a. Measured pressure spectral density around the circumference of a vertical cylinder (narrow band).

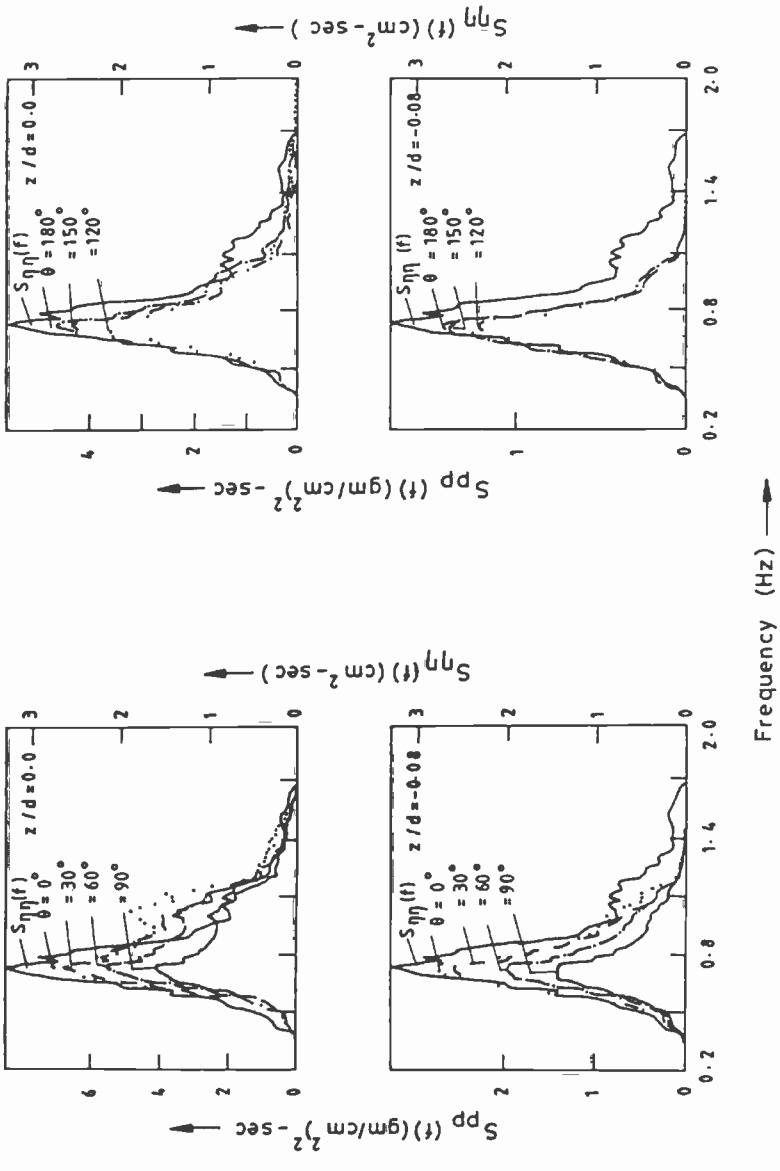

FIG. 6b. Measured pressure spectral density around the circumference of a vertical cylinder (PM1).

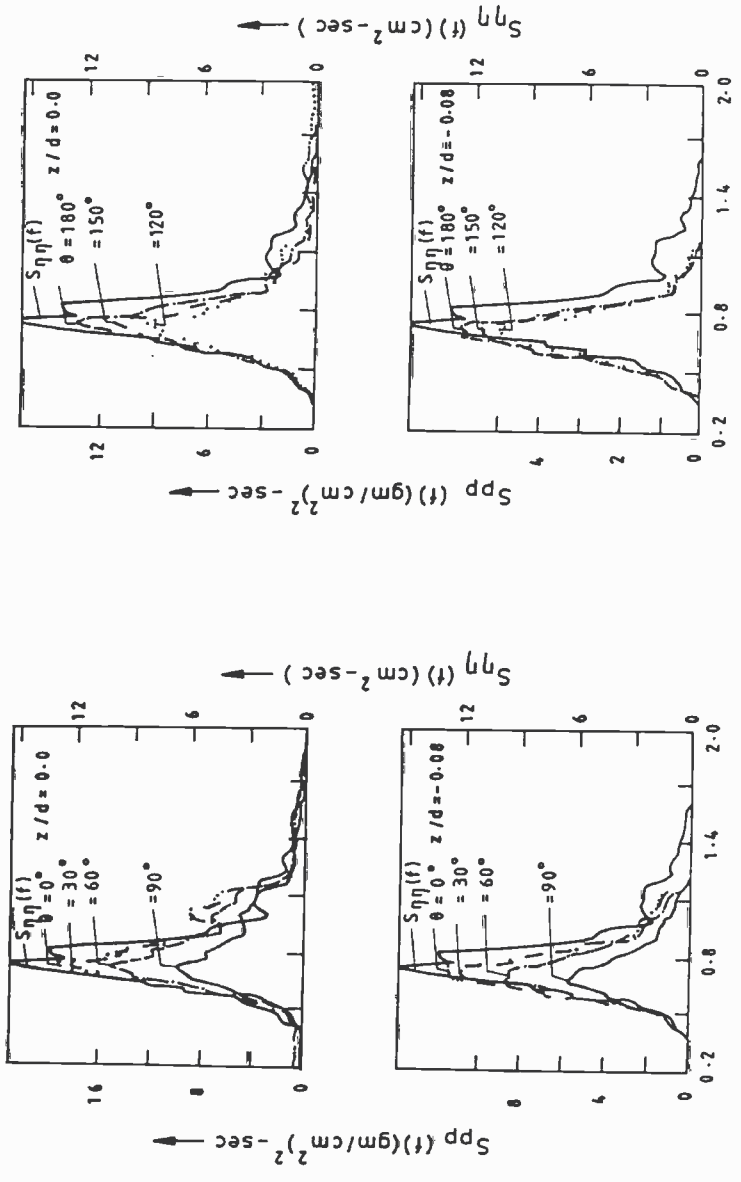

FIG. 6c. Measured pressure spectral density around the circumference of a vertical cylinder (PM2).

that the dynamic pressure around the circumference of the test cylinder at any depth of submergence decreases with increase in the value of θ from 0 to 120°, beyond which there is an increase in the pressure spectral density. It is to be noted from Figs 6b and c that the measured pressure spectra at S.W.L. for the PM1 and PM2 cases show secondary peaks for θ = 0–90° at frequencies beyond 1 Hz, which are absent for the case of narrow band spectra. It reveals that the pressure transducers at θ = 0–90° are mostly exposed to the direct impact of the incident waves and the effect of diffraction is more pronounced beyond 1 Hz, whereas at θ = 90–180°, (being the shadow region), the pressure transducers in this region are expected to sense the dynamic pressures after the waves get scattered by the cylinder, especially at higher frequencies. This explains the reason for the presence of secondary peaks at S.W.L. for θ = 0–90° beyond 1 Hz and its absence for θ = 120–180° even beyond 1 Hz. It is also noticed from these plots that the circumferential variation of the spectral density of the dynamic pressure is quite large from θ = 30–90°, when compared to that from θ = 120–180°.

4.4. *Theoretical and experimental peak pressure spectral values*

A plot showing the theoretical and measured spectral peak values of the dynamic pressures around the circumference of the test cylinder at different elevations (z/d = 0.0 to − 0.26) for all the incident wave spectra referred to in Table 1 are shown in Fig. 7. The correlation between the theoretical and measured peak pressure spectral values

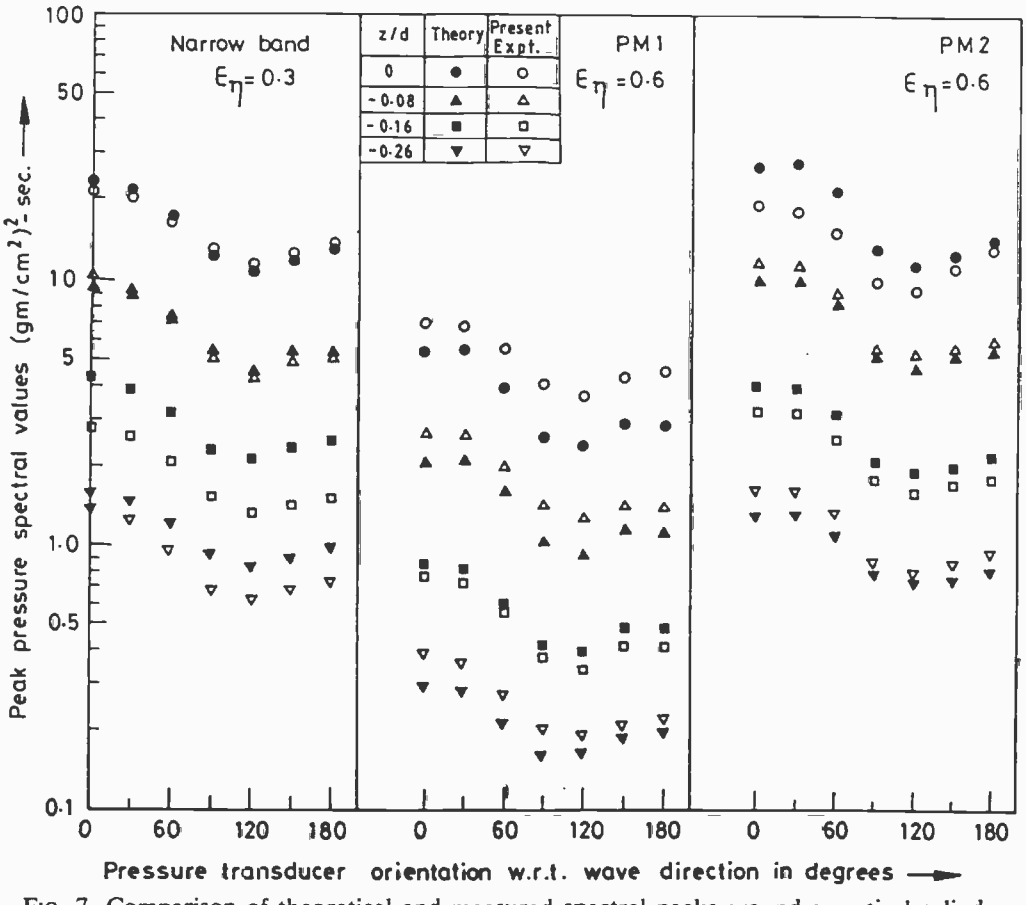

FIG. 7. Comparison of theoretical and measured spectral peaks around a vertical cylinder.

is found to be good even at S.W.L. for the case of narrow band spectra, whereas deviations are observed in the case of PM1 and PM2 at S.W.L. This is due to the dominant diffraction and nonlinear effects existing for the case of broad band spectra as discussed in Section 4.2.

4.5. *Theoretical and measured zeroth pressure spectral moment*

In order to visualise clearly the total energy of the dynamic pressure induced at different elevations due to the three different incident wave spectra mentioned in Table 1, a comparative plot showing the theoretical and measured zeroth pressure spectral moment is given in Fig. 8. The zeroth moment at any elevation is a maximum at $\theta = 0°$ and decreases as θ increases up to 120°, beyond which it increases slightly. The correlation between the theory and experiments, in general, is found to be good. Here again it is seen that at $z/d = -0.36$, the total measured pressure energy observed is less than 1% of that observed at S.W.L. as mentioned earlier. The deviation between the measured and theoretical zeroth moment of the dynamic pressure at $z/d = -0.36$ is greater. Such a phenomenon has also been observed by Raman and Rao (1983) and Caveleri *et al.* (1977).

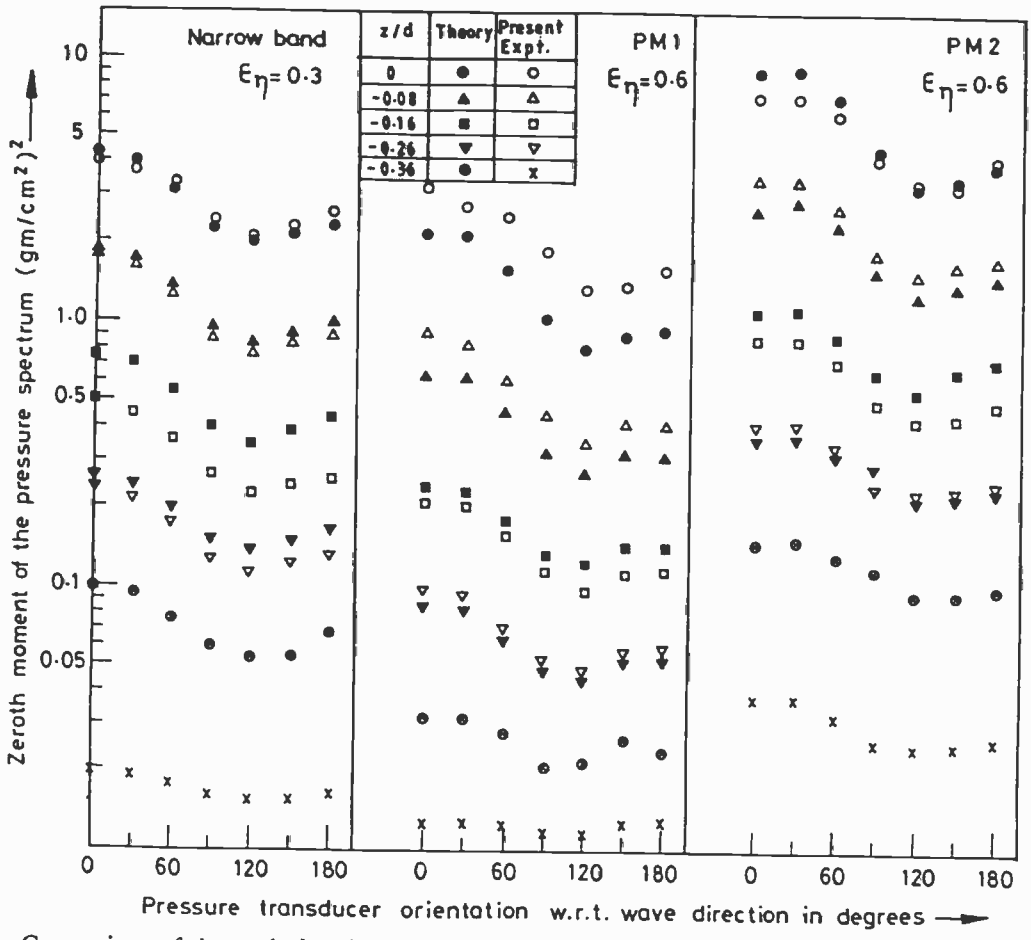

FIG. 8. Comparison of theoretical and measured zeroth moment of the pressure spectrum around a vertical cylinder.

4.6. *Theoretical and measured spectral width parameters of dynamic pressures*

The spectral width parameter, ϵ_p for the dynamic pressure is given as

$$\epsilon_p = \sqrt{\left(1 - \frac{m_2^2}{m_0 m_4}\right)} \tag{9}$$

where m_n denotes the nth spectral moment and is given by

$$m_n = \int_0^\infty S_{pp}(f) f^n \mathrm{d}f. \tag{10}$$

The variation of the theoretical and experimental ϵ_p around the circumference of the cylinder for different z/d, for PM1 and narrow band spectra, is shown in Fig. 9. Since ϵ_p for both PM1 and PM2 are nearly the same, only PM1 has been considered.

The general correlation between the experimental and theoretical ϵ_p is found to be satisfactory for z/d up to -0.26, beyond which large deviations of experimental values from the theory are observed. This discrepancy may be attributed to the fact that at lower levels in deep water, as seen earlier, the magnitude of dynamic pressure is very small, and a slight error in their measurement would get magnified considerably in the calculation of the fourth spectral moment leading to the possible increase in ϵ_p. It is seen that the theoretical and experimental ϵ_p are almost constant around the circumference of

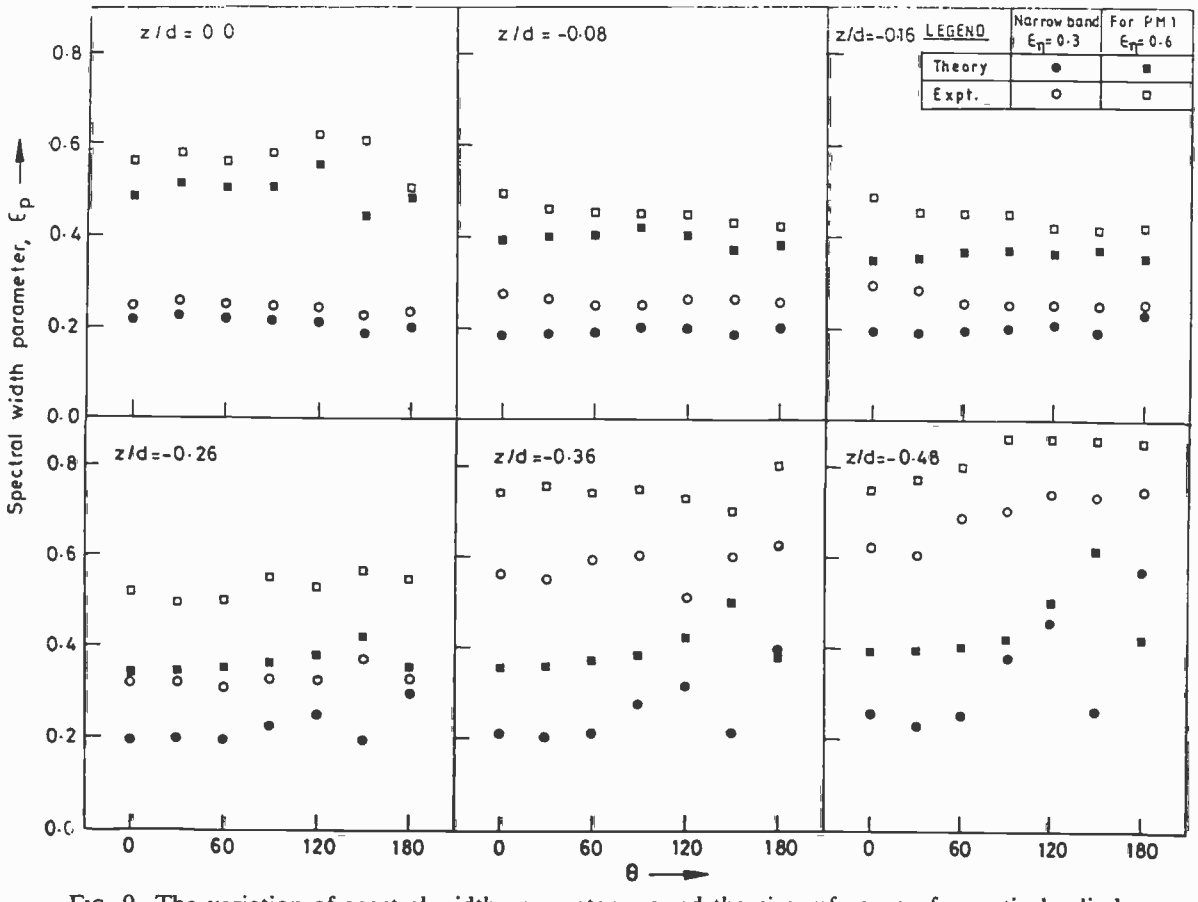

FIG. 9. The variation of spectral width parameter around the circumference of a vertical cylinder.

the cylinder for z/d up to -0.26, beyond which dominant variation in ϵ_p is observed especially for $\theta > 60°$.

A typical plot showing the correlation of theoretical and experimental ϵ_p along the depth for three different θ values ($\theta = 0°$, $90°$ and $180°$) for both narrow band and PM1 spectra is depicted in Fig. 10. It is seen from this plot that the correlation between the theoretical and experimental ϵ_p values are better for the narrow band spectrum than for the PM1 spectrum up to $z/d = -0.26$. The reason for the deviations between the theory and the experiments for z/d beyond -0.26 has been discussed earlier.

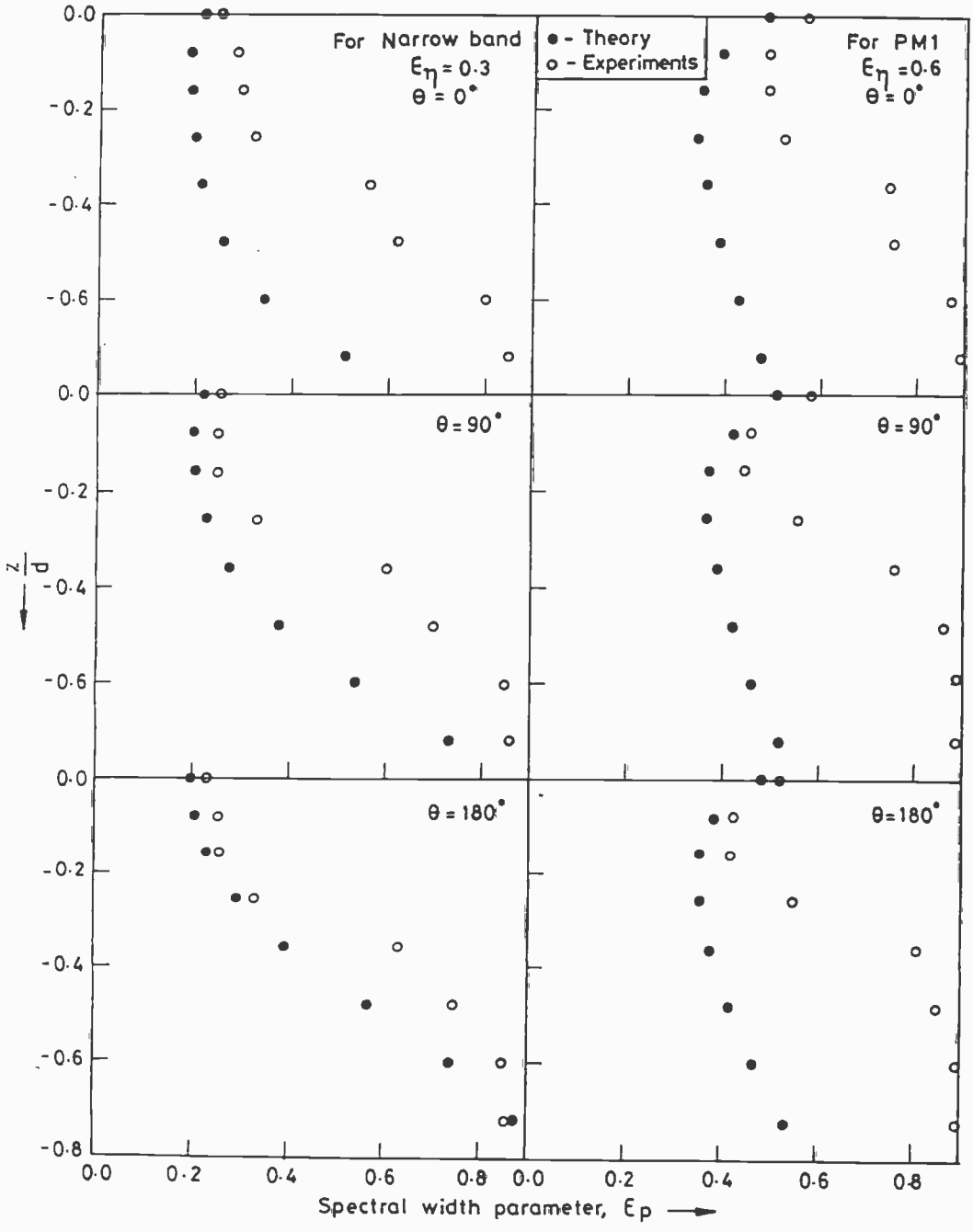

FIG. 10. Variation of spectral width parameter along the depth of a vertical cylinder.

4.7. *Comparison of regular and random wave results*

The comparison of normalised pressures C_p (see Section 2.2.) as a function of θ for different *z/d* values based on regular and random wave tests is shown in Fig. 11. In the case of random waves, the scattering parameter *ka* was computed using peak spectral frequency. The wave frequency of the regular wave could not be matched with this exactly due to the experimental limitations. The normalised pressures C_p from the random wave tests with PM1, PM2 and narrow band spectra were obtained as discussed in Section 2.2. The theoretical plots of C_p obtained using the MacCamy and Fuchs linear diffraction theory (1954) are also superposed on these plots. It is seen that the experimental results, from both regular and random wave tests, deviate from the theory for the transducer location at S.W.L. This deviation is observed to be more pronounced

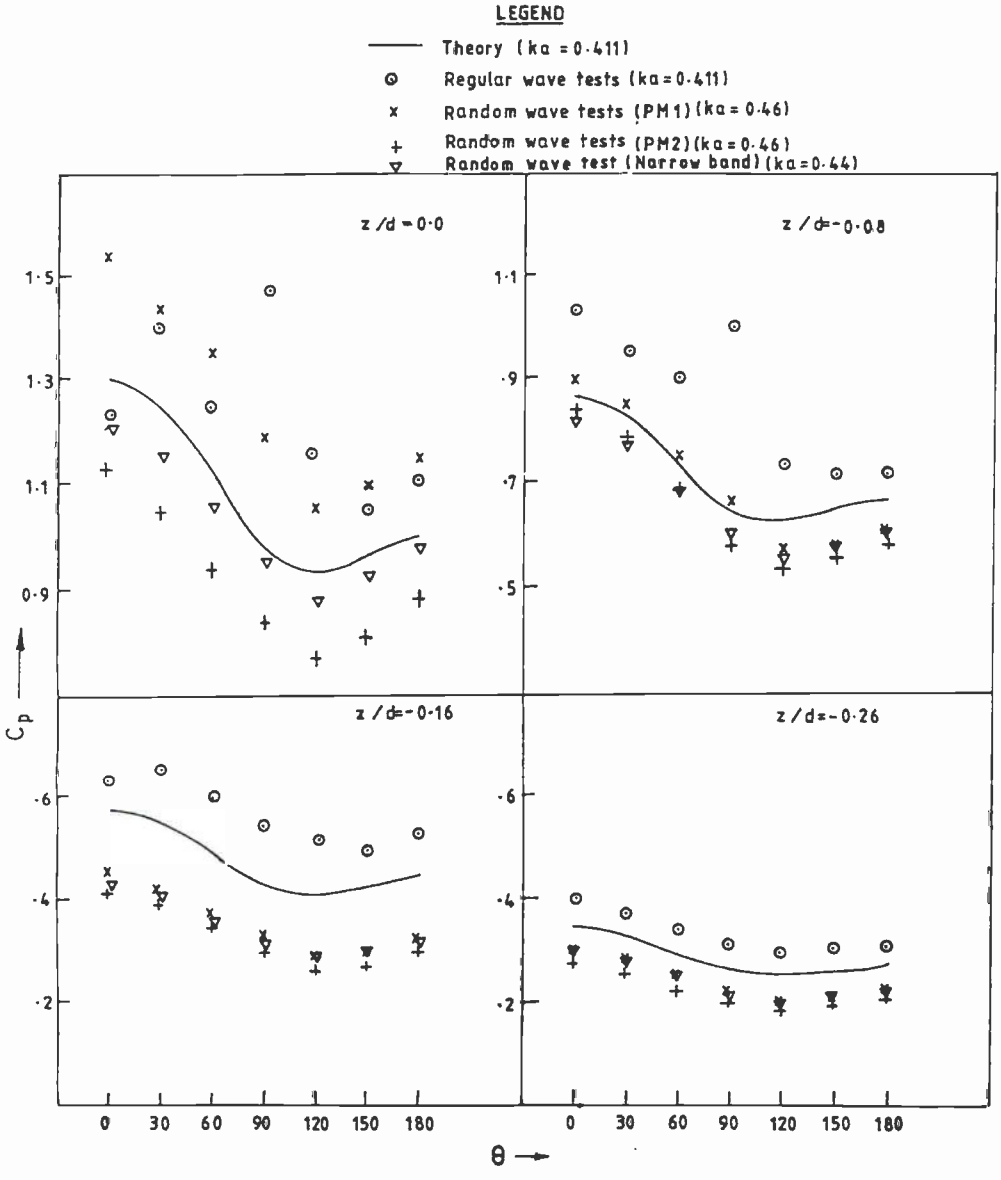

FIG. 11. Comparison of regular and random wave pressure results.

for $\theta = 90°$ for the case of regular waves, whereas this is not so for the random wave pressure tests. This may be due to the fact that the wave reflection from the side wall for the case of a monochromatic wave establishes its presence, whereas for random waves, since it is a combination of many frequency components, the effect of the reflected waves from the side wall gets nullified by the scattering waves from the cylinder. It is seen that the regular wave tests yielded consistently higher values of C_p than the theory, whereas the opposite trend is noticed in the case of random wave pressure tests. This can partly be attributed to the fact that the average pressure coefficient C_p is assumed to be constant over the whole range of frequencies and also the small difference in the ka value considered for comparison (ka = 0.411, 0.44 and 0.46 for regular wave, narrow band and for the two PM spectra, respectively). It is interesting to note that the agreement between the MacCamy and Fuchs theory and the experimental results for C_p obtained for the narrow band spectrum is found to be good even at S.W.L., unlike the results from the PM1 and PM2 spectra. It is observed that the C_p values for the case of a narrow band spectrum for z/d below − 0.08 almost coincide with the results for the PM1 spectrum.

4.8. *Incident and diffracted wave spectra*

4.8.1. *Comparison between theory and experimental values.* In order to study the pattern of the diffraction by the test cylinder, six different locations around the cylinder (viz., D1–D6 as shown in Fig. 12) were chosen to measure the time history of the

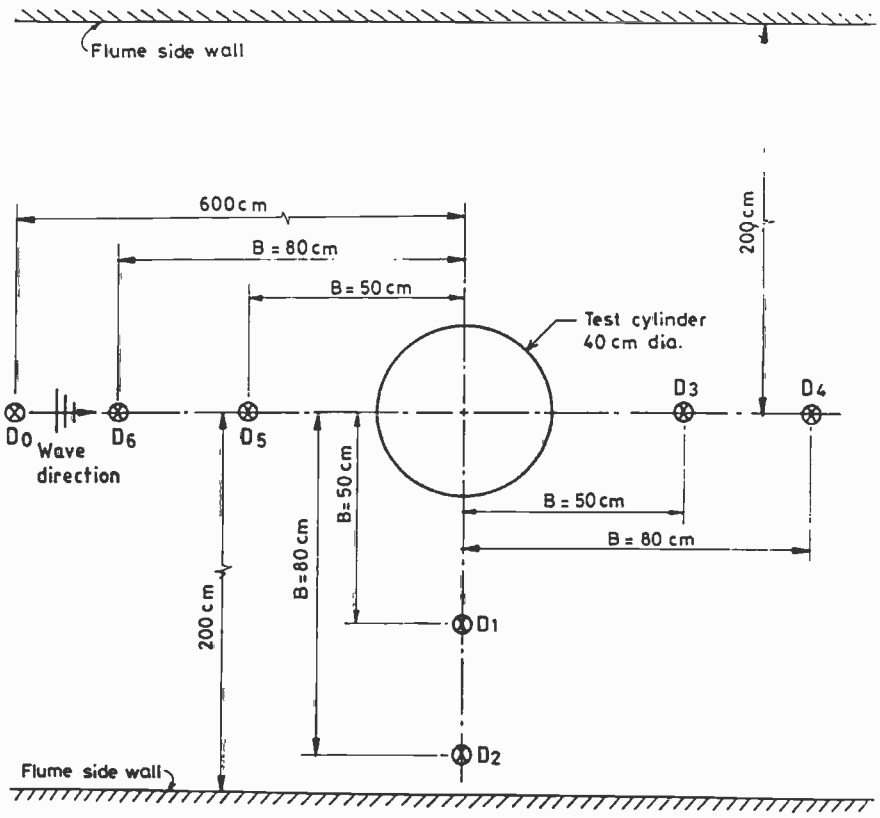

FIG. 12. Location details of the diffracted wave probes.

diffracted wave elevation. B/D values of 1.25 and 2 have been used, where B is the distance of the wave gauge from the centre of the test cylinder and D is the diameter of the cylinder. Though experiments were conducted for all the three spectra given in Table 1, only selected cases are taken up for discussion.

The comparison of the theoretical and the measured diffracted wave spectra for the narrow band case, for locations D1, D2, D3 and D5, are shown in Fig. 13a. The first two locations are considered in preference to D4 and D6 in order to examine the possible side wall effects. The corresponding incident wave spectrum is also superposed on these plots. It is seen that for all these four locations the diffracted wave energy is greater than that of the incident wave energy. The agreement between the theory [Equation (6)] and the experiments are found to be satisfactory. However, the deviations observed especially near the spectral peak may be due to the nonlinear effects, which are not accounted for in the theory.

In order to demonstrate the effect of wave steepness, wave elevation spectra at locations D1–D6 for PM1 and PM2 cases are shown in Figs 13b–d, which reveals that the diffracted wave energy is greater than the corresponding incident wave energy as observed in the narrow band case. It is surprising to note from these figures that the deviation between the measured and theoretical diffracted wave energy is smaller for the case of PM2 (larger energy level) when compared to the case of PM1 (smaller energy level), consistently for all the locations considered. Based on the foregoing discussions, it is inferred that the correlation between the theoretical and measured diffracted wave spectra for the case of the narrow band spectrum is better than in the case of the two broad band spectra considered in this study.

4.8.2. *Diffracted wave spectrum around the cylinder.* The trends in the variation of the diffracted wave energy around the cylinder at the locations discussed in the earlier section for the three incident wave spectra were similar. Hence, only a representative plot showing the variation of the measured spectral density of the diffracted waves corresponding to the narrow band case is shown in Fig. 14 for B/D of 1.25 and 2.0. As seen earlier the diffracted wave energy is significantly higher compared to the incident wave energy. The diffracted wave energy is found to be maximum at location D5, apparently due to the build-up of scattered waves in front of the cylinder around this location.

4.8.3. *Theoretical and measured zeroth moment and peak values of the diffracted wave spectra.* A comparison of the theoretical and the measured zeroth moment and peak values of the diffracted wave spectrum at selected locations around the cylinder is shown in Fig. 15. As discussed earlier, the zeroth moment and the spectral peak of the three incident wave spectra are smaller than the respective values of the diffracted wave. It is seen consistently that the zeroth moment and the spectral peak are a maximum at location D5. It is also noticed that the measured zeroth moment and the spectral peak is a minimum at location D6. A study of the above two parameters show that the B/D value does not significantly influence the diffracted wave energy behind the cylinder when compared to the locations in front of the cylinder. Similarly the above two parameters are almost identical for locations D1 and D2 near the side wall, except that an increase in their values is noticed at D2 for the incident wave spectrum

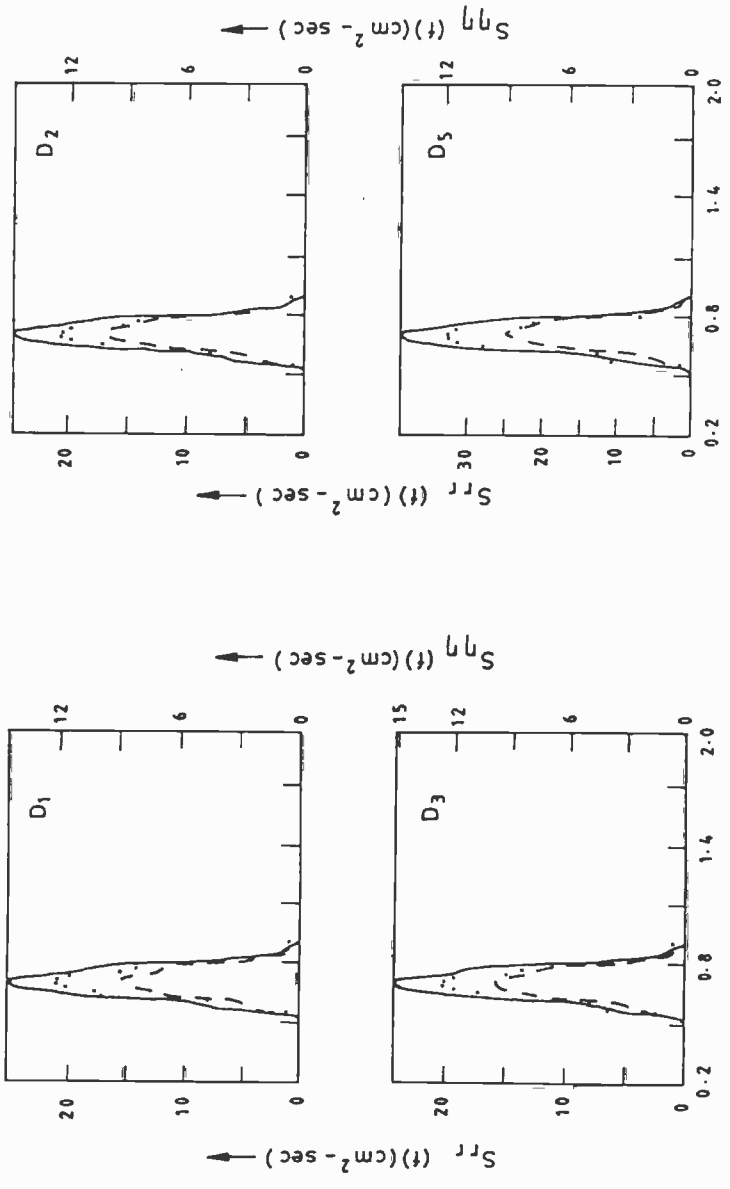

FIG. 13a. Comparison of theoretical and experimental diffracted wave spectrum (narrow band).

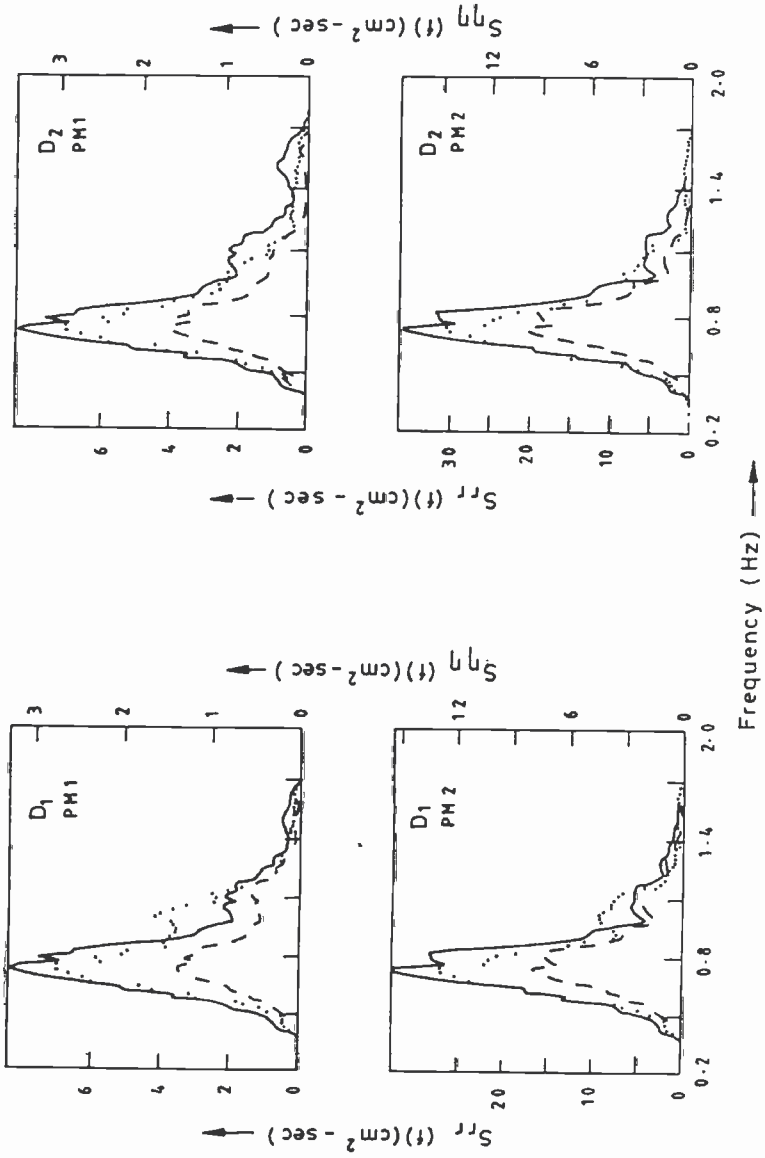

FIG. 13b. Comparison of theoretical and experimental diffracted wave spectrum.

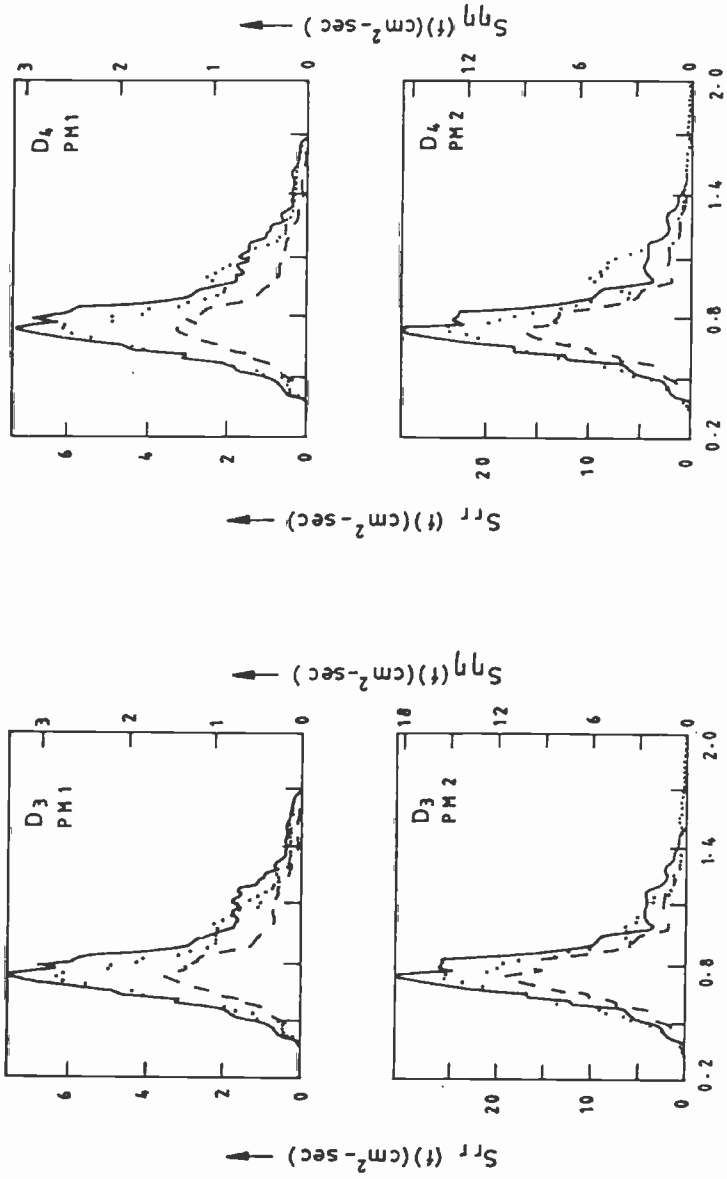

FIG. 13c. Comparison of theoretical and experimental diffracted wave spectrum.

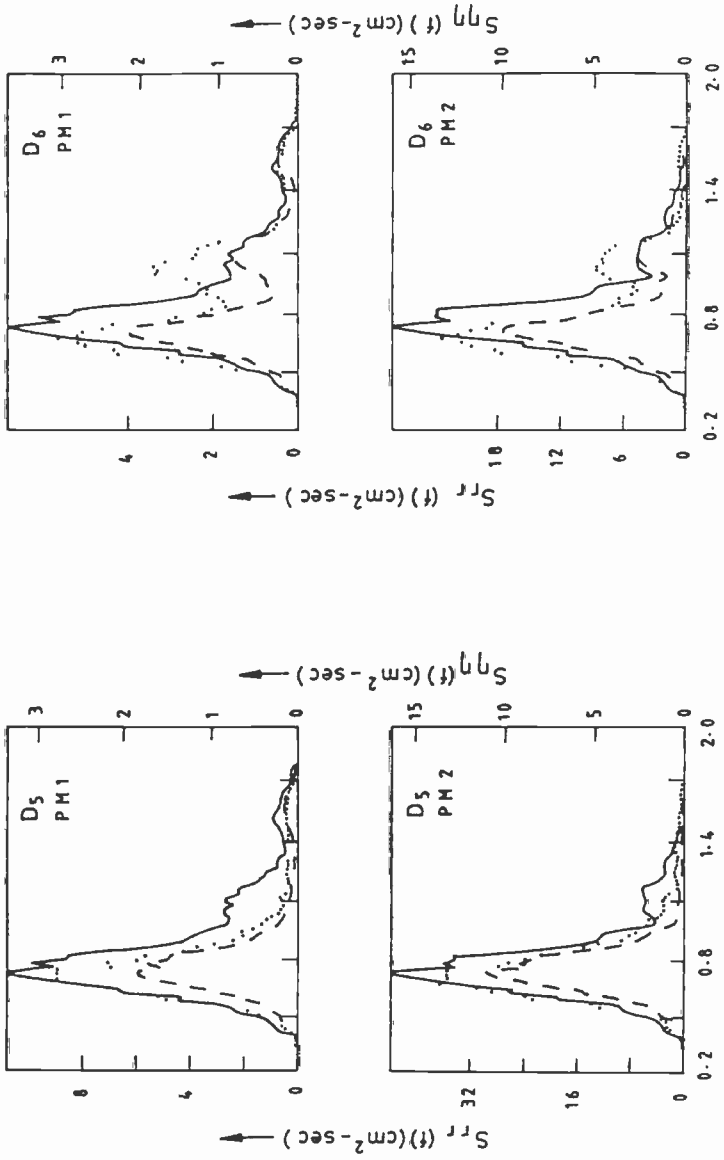

FIG. 13d. Comparison of theoretical and experimental diffracted wave spectrum.

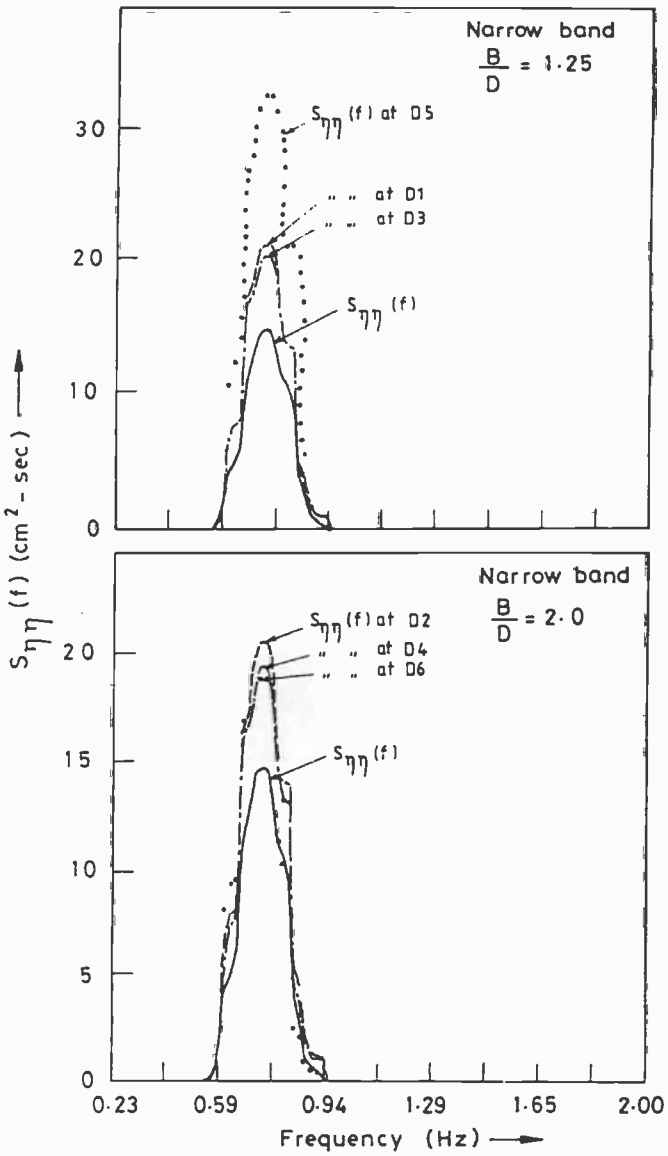

FIG. 14. Comparison of measured incident and diffracted wave elevation spectrum.

PM2 (higher energy level), since the reflections from the side wall are expected to be greater for steeper waves. Based on the percentage difference of the measured values of the zeroth moment and the peak spectral value from their respective theoretical values, it is found that the agreement between the theory and experiments for both these parameters is better for the case of a narrow band spectrum as compared to the broad band incident wave spectra.

5. CONCLUSIONS

The hydrodynamic pressures exerted around a vertical cylinder due to regular and random waves were measured in a wave flume. The diffracted wave field around the cylinder at six different locations was measured. The measured spectral density of the

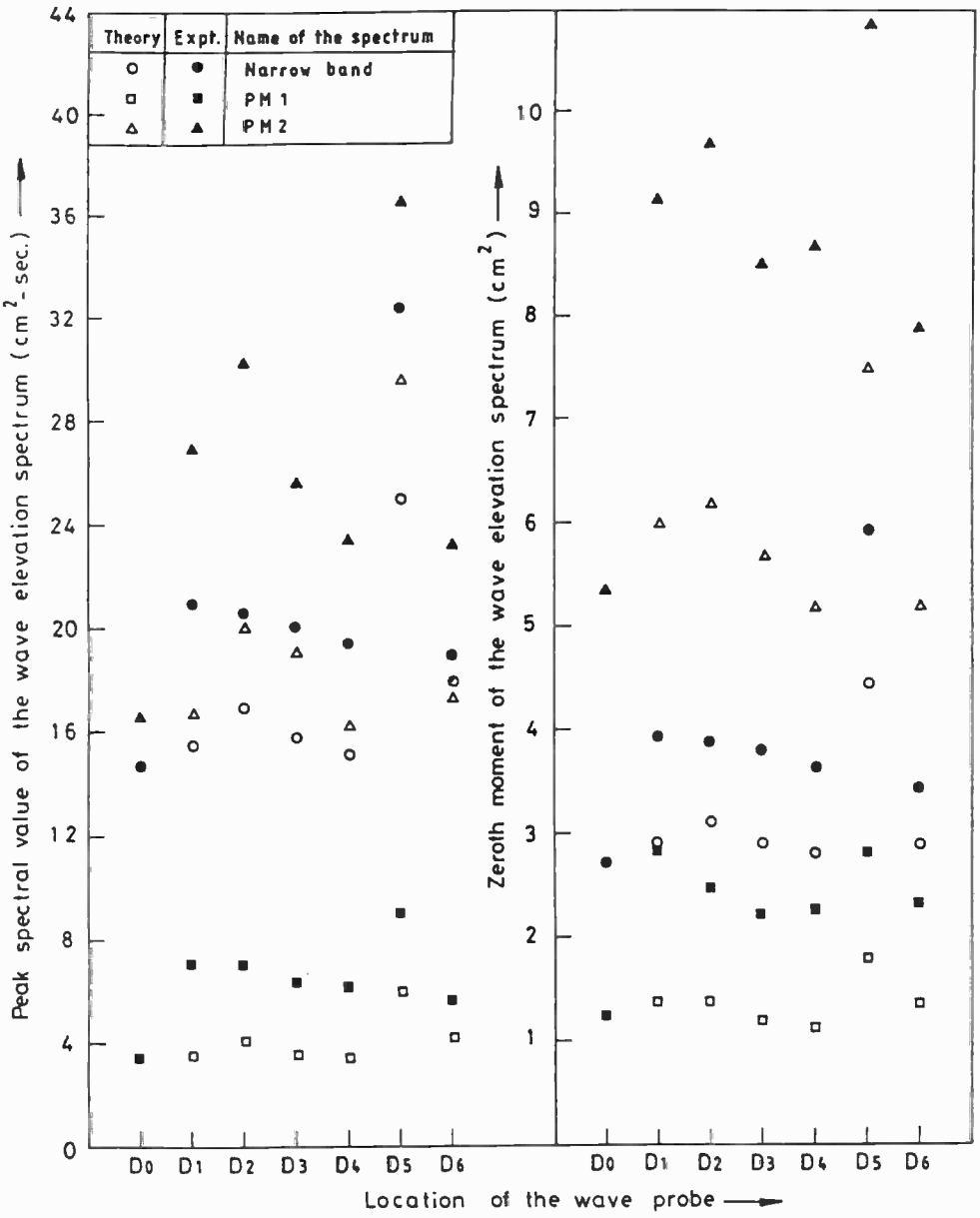

FIG. 15. Variation of spectral peak and zeroth moment of incident and diffracted wave field.

dynamic pressure and the diffracted wave elevation around the cylinder is compared with a theoretical formulation based on the MacCamy and Fuchs linear diffraction theory. The following conclusions have been drawn based on the present study:

(1) The agreement between the measured and theoretical pressure spectrum exerted on a vertical cylinder is found to be better for a narrow band incident wave spectrum when compared to a broad band case.

(2) The spectral peaks of the dynamic pressure of both experiments and theory shift towards the lower frequency region as the absolute of the relative depth of submergence of the pressure transducer $|z/d|$ increases.

(3) For any z/d, the spectral peak of the dynamic pressure around the circumference of the cylinder reduces with the increase in θ from 0 to 120°, beyond which it increases slightly.
(4) The circumferential variation of the peak of the dynamic pressure is quite large from θ = 30–90° when compared to the same from θ = 120–180°.
(5) The agreement between the theoretical and experimental spectral width parameter of the dynamic pressure spectrum is found to be good up to $z/d = -0.26$, beyond which deviations are observed.
(6) The correlation between the regular wave test and the random wave test based on the average pressure coefficient applied over the frequency domain is found to be encouraging.
(7) The side wall reflection is more dominant for the regular waves when compared to the random waves.
(8) The diffracted wave energy around the cylinder for the selected locations is found to be more than the incident wave energy.
(9) The experimental diffracted wave spectrum overestimates the corresponding theoretical value by around 15%.
(10) The spacing parameter B/D has a significant influence on the measured spectral peak and zeroth moment of the diffracted wave spectrum in front of the cylinder, whereas its influence on the said parameters for the wave field behind as well as in phase with the cylinder is insignificant.

REFERENCES

CAVELERI, L., EWING, J.A. and SMITH, N.D. 1977. Measurement of the pressure and velocity field below surface waves. In *Turbulent Fluxes through Sea Surfaces, Wave Dynamics and Prediction*, FAVRE, A. and HASSELMANN, K. (eds), pp. 257–273. Plenum Press, New York.

CHAKRABARTI, S.K. and TAM, A. 1975. Interaction of waves with large vertical cylinder. *J. Ship Res.* **19**, 22–33.

CHAKRABARTI, S.K., LIBBY, A.R. and KOMPARE, D.J. 1986. Dynamic pressures around a vertical cylinder in waves. *Proceedings of the Offshore Technology Conference, Houston, Texas, 5–8 May*, OTC 5102, pp. 193–199.

DAEMRICH, K.F., EGGERT, W.D. and KOHLHASE, S. 1980. Investigation on irregular waves in hydraulic models. *Proceedings of the Coastal Engineering Conference, Sydney, 23–28 March*, pp. 186–203.

ENDO, R. and TOSAKA, N. 1985. On the wave pressure distributions acting on offshore cylindrical shell structures. *Proceedings of the Ocean Space Utilisation, Nihon University, Tokyo, 9–12 June*, pp. 117–124. Springer-Verlag, Tokyo.

HAVELOCK, T.H. 1940. The pressure of water waves on a fixed obstacle. *Proc. R. Soc. Lond.* **A175**, 409–421.

HELLSTORM, B. and RUNDGREN, L. 1954. Model tests on Deland Soedra Grund lighthouse. Bulletin No. 39. The Institute of Hydraulics, Royal Institute of Technology, Stockholm, Sweden.

LAIRD, A.D.K. 1955. A model study of wave action on a cylindrical island. *Trans. Am. geophys. Un.* **36**, 279–285.

MACCAMY, R.C. and FUCHS, R.A. 1954. Wave forces on piles: a diffraction theory. U.S. Army Beach Erosion Board, Technical Memorandum No. 69, Washington, D.C.

MORISON, J.R., O'BRIEN, M.P., JOHNSON, J.W. and SCHAFF, S.A. 1950. The forces exerted by surface waves on piles. *Petroleum Transactions, AIME*, **189**, 149–154.

NAKAMURA, H. 1976. Wave pressures on large circular cylindrical structures. *Proceedings of Coastal Engineering*, Honolulu, pp. 2290–2300.

PRIEST, M.S. 1962. Shallow water wave action on a vertical cylinder. *J. WatWay, Harbour Coastal Engng Div., ASCE*, **88**, No. WW2, 1–9.

RAMAN, H. and SAMBHU VENKATA RAO, P. 1983. Dynamic pressure distribution on large cylinders caused by wind generated random waves. *Ocean Engng* **10**, 749–786.